
Article:
Zhou, L. orcid.org/0000-0001-7760-832X, Dong, X. orcid.org/0009-0002-6584-9526, Qiu, K. orcid.org/0000-0003-0355-284X et al. (3 more authors) (2025) Ray-based characterization of the AMPLE model from 0.85 to 5 GHz. IEEE Transactions on Antennas and Propagation, 73 (10). pp. 8174-8188. ISSN: 0018-926X

https://doi.org/10.1109/tap.2025.3589793

Ray-Based Characterization of the AMPLE Model from 0.85 to 5 GHz

Lingyou Zhou, *Graduate Student Member, IEEE,* Xin Dong, *Graduate Student Member, IEEE,* Kehai Qiu, *Member, IEEE,* Gang Yu, *Graduate Student Member, IEEE,* Jie Zhang, *Senior Member, IEEE,* and Jiliang Zhang, *Senior Member, IEEE*

***Abstract*—In this article, we characterize the adaptive multiple path loss exponent (AMPLE) radio propagation model under urban macrocell (UMa) and urban microcell (UMi) scenarios from 0.85 to 5 GHz using Ranplan Professional. We first enhance the original AMPLE model by introducing an additional frequency coefficient to support path loss prediction across multiple carrier frequencies. By using measurement-validated Ranplan Professional simulator, we simulate four cities and validate the simulations for further path loss model characterization. Specifically, we extract the close-in (CI) model parameters from the simulations and compare them with parameters extracted from measurements in other works. Under the ray-based model characterization, we compare the AMPLE model with the 3rd Generation Partnership Project (3GPP) path loss model, the CI model, the alpha-beta-gamma (ABG) model, and those with simulation calibrations. In addition to standard performance metrics, we introduce the prediction-measurement difference error (PMDE) to assess overall prediction alignment with measurement and mean simulation time per data point to evaluate model complexity. The results show that the AMPLE model outperforms the existing models while maintaining similar model complexity.**

***Index Terms*—Path loss, prediction, radio propagation, ray tracing.**

I. Introduction

CHANNEL modeling in sixth generation (6G) and beyond systems will need to address significantly more complex propagation scenarios across a wider range of frequencies [1], [2], [3]. As one of the key large-scale parameters (LSPs), path loss and radio propagation modeling play a crucial role in the statistical channel models, as they constrain the overall channel modeling process, including the prediction of small-scale parameters (SSPs) and the construction of the channel matrix [4], [5], [6], [7], [8], [9], [10], [11], [12], [13]. In other words, to further enhance the statistical channel models based on current efforts, neglecting LSPs like path loss and focusing solely on SSPs will lead to half the result with twice the effort [14].

Currently, deterministic models and empirical models are the two main types for radio propagation path loss predictions. For deterministic models, they are either based on the full-wave solutions, such as finite-difference time domain (FDTD) [15], finite element method (FEM), method of moments (MOM) [16], and finite integration technique (FIT); or ray-based methods, such as the ray-tracing and ray-launching methods [17], [18]. Since the full-wave solutions are significantly more complex and primarily used for detailed channel modeling, deterministic models for path loss prediction typically refer to the ray-based models only. Based on ray-optics, those ray-based models predict path loss by incorporating detailed environmental information and simulating the full propagation process. By applying Maxwell's equations with appropriate boundary conditions, they simulate the entire propagation channel, with path loss obtained as part of the modeling outcome. However, when path loss is the main outcome of interest, the requirements for detailed environmental data combined with the complexity of solving electromagnetic equations make these models difficult to deploy across diverse propagation scenarios [19].

In contrast, for simplicity, empirical models predict path loss using a small set of parameters extracted from measurements and/or ray-based simulations under different scenarios. Initially, empirical models such as the Okumura-Hata model, the European Cooperation in Science and Technology (EURO-COST) research COST-231 model [20], and the Stanford University Interim (SUI) model [21], are proposed for their simplicity and fast computation. However, they only cover limited scenarios and often result in large prediction errors. To achieve both simplicity and accuracy in general path loss prediction, geometry-based stochastic channel models (GSCMs) construct path loss models extracted from measurements and/or ray-based simulations under different scenarios [4], [5], [6], [7], [8], [9], [10], [11], [12], [13]. Those models include the

This work was supported in part by the Horizon Europe and Innovation Program under Grant 101086219; in part by the UK EPSRC under Grant EP/X038971/1; and in part bt the Open Research Fund of National Mobile Communications Research Laboratory, Southeast University under Grant 2024D09. *(Corresponding Author: Jie Zhang)*

Lingyou Zhou is with the School of Electrical and Electronic Engineering, The University of Sheffield, Sheffield, S10 2TN, U.K.

Xin Dong is with the School of Electrical and Electronic Engineering, The University of Sheffield, Sheffield, S10 2TN, U.K., and also with the R&D Department, Ranplan Wireless Network Design Ltd., Cambridge, CB23 3UY, U.K.

Kehai Qiu is with the Department of Computer Science and Technology, University of Cambridge, Cambridge, CB3 0FD, U.K.

Gang Yu is with the School of Electrical and Electronic Engineering, The University of Sheffield, Sheffield, S10 2TN, U.K., and also with 5G/6G Innovation Centre, University of Surrey, Surrey, GU2 7XH, U.K.

Jie Zhang is with the R&D Department, Cambridge AI+ Ltd., Cambridge, CB23 3UY, U.K., and also with the R&D Department, Ranplan Wireless Network Design Ltd., Cambridge, CB23 3UY, U.K.

Jiliang Zhang is with the State Key Laboratory of Synthetical Automation for Process Industries and the College of Information Science and Engineering, Northeastern University, Shenyang, 110819, China, and also with the National Mobile Communications Research Laboratory, Southeast University, Nanjing, 210096, China.

Digital Object Identifier 10.1109/TAP.2025.3589793

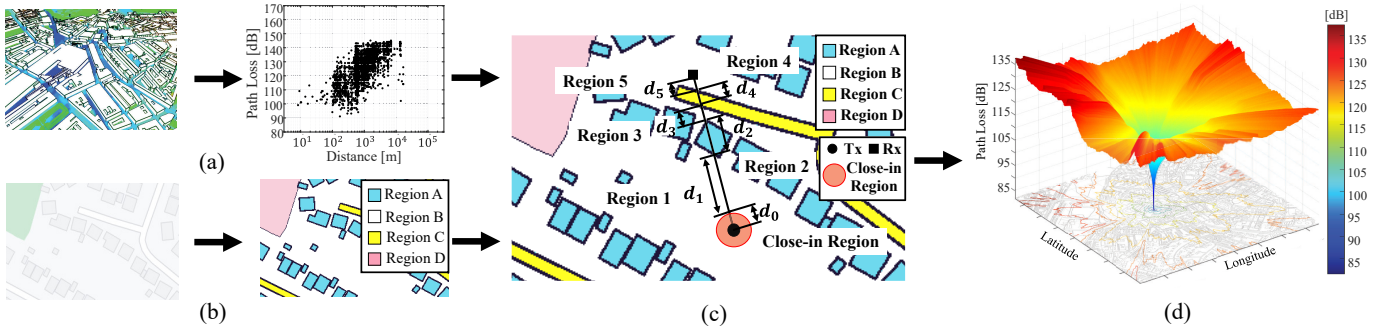

Fig. 1. Example of the AMPLE model construction process [14]. (a) Simulation/measurement collection and analysis. (b) Environment collection and classification. (c) Straight line construction. (d) Parameter extraction and path loss prediction.

alpha-beta-gamma (ABG) model, the close-in (CI) free space reference distance model, and the CI model with a frequency-dependent path loss exponent (PLE) (CIF) [6], [22]. Still, without redesigning the model structures, these models are limited by their lack of environmental considerations, which gradually leads to large prediction errors as environmental complexity increases.

To cover propagation environments with low computational complexity, we previously proposed a fast adaptive multiple path loss exponent (AMPLE) model, and validated using both measurements [14] and ray-based simulations [23]. To enable practical deployment of the AMPLE model, in this article, we characterize the AMPLE model under the urban macrocell (UMa) and the urban microcell (UMi) scenarios from 0.85 to 5 GHz using Ranplan Professional. The main contributions of this article are as follows.

- Based on our previous works [14], [23], [24], we enhance the AMPLE model by introducing an additional frequency coefficient to support path loss prediction across different carrier frequencies.
- We use Ranplan Professional, a measurement-validated ray-based simulator, to simulate and collect path loss data for fifth generation new radio (5GNR) 0.85 GHz, 2.1 GHz, and 5 GHz under UMa and UMi scenarios. Four cities are selected as propagation environments to set up the simulations, and the basic information including environments and propagation is based on the definitions of the typical UMa and UMi scenarios [4], [6], [22].
- We conduct a simple validation for the ray-based simulations, specifically under the field of path loss model characterization. That is, we extract the CI model parameters from the simulations including UMa line-of-sight (LOS), UMa non-line-of-sight (NLOS), and UMi NLOS environments. Then, we compare the simulation-based parameters with those extracted from measurements reported by the research group of Theodore S. Rappaport in [22]. The comparison results show close alignment between the simulation-based and measurement-based CI model parameters.
- We characterize and validate the AMPLE model using Ranplan simulation data across the 0.85–5 GHz range for the UMa LOS, UMa NLOS, UMi LOS, and UMi NLOS environments. The whole characterization and validation process is given, which can be considered as the standard characterization process of the AMPLE model for future research.
- We compare the AMPLE model with the current path loss models in the 3rd Generation Partnership Project (3GPP) [4] and 5G Channel Model Simulation Group (5GCMSIG) [6] under the UMa/UMi scenarios with LOS/NLOS environments. Beyond general metrics such as root mean square error (RMSE) and mean absolute error (MAE), we propose prediction-measurement difference error (PMDE) to show overall alignment between predictions and measurements, and the mean simulation time per point to show model complexity. The overall results show that the AMPLE model outperforms the current empirical models by considering environments while maintaining similar model complexity.

The remainder of this article is organized as follows. Section II introduces the enhanced AMPLE model considering propagation carrier frequencies. Section III presents the ray-tracing simulations conducted using the measurement-validated Ranplan Professional. In Section IV, the characterization process of the AMPLE model from 0.85 to 5 GHz is given, along with a performance comparison against other models. In Section V, a brief discussion of the AMPLE model is given. Finally, conclusions are drawn in Section VI.

II. The AMPLE Model

In this section, we give a brief background of the AMPLE model we previously proposed [14], [23], [24]. And we also refine the AMPLE model by further considering propagation carrier frequency. An example of the model construction process is shown in Fig. 1.

A. Preliminary Information

To construct the AMPLE model, both path loss and scenario information are necessary during the model construction stage [14]. For path loss data, similar to other empirical path loss models [4], [5], [6], [22], preliminary path loss data under the desired scenario are collected from ray-based simulations and/or measurements, as illustrated in Fig. 1(a). After that, to combine the environment information and construct a site-specific model, the map information of the scenario is another

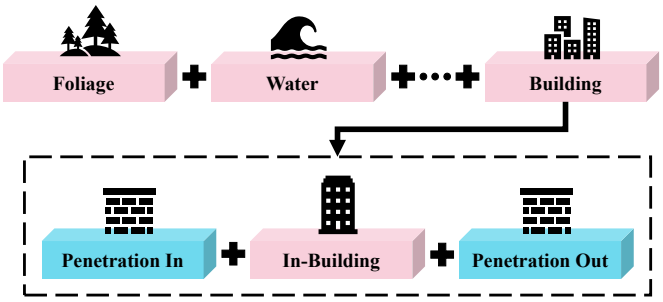

Fig. 2. Example of building penetration loss.

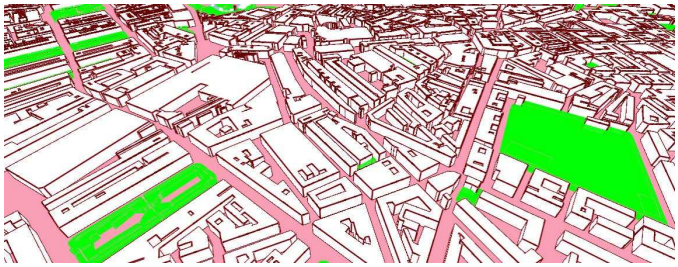

Fig. 3. Example of the Ranplan Professional outdoor simulation in London.

preliminary model characterization condition. As shown in Fig. 1(b), the AMPLE model utilizes the two-dimensional (2D) region map to cover environment information, of which it classifies the whole map into different region types. By using manual classification, map classification based on image processing, or artificial intelligence (AI)-based classification methods, the environment maps collected from satellite systems, digital map systems, and geographic information system (GIS) can be therefore transformed.

To combine path loss and map information, each type of region is assigned with a PLE, and a straight line between each transmitter-receiver (T-R) link is generated. The straight line records the intersected region PLE as well as the corresponding region length, which can be expressed as [14], [23]

$$\mathbf{S}_z = \begin{bmatrix} n_0 & n_1 & n_2 & \cdots & n_{R_z} \\ d_0 & d_1 & d_2 & \cdots & d_{R_z} \end{bmatrix}, \tag{1}$$

where $\mathbf{S}_z$ is the line matrix of the zth T-R link, n_{R_z} is the PLE of the R_zth region, and d_{R_z} is the corresponding region length. For common practice [20], [25], we define regions within d_0 as the CI region, where d_0 is the CI distance [14], [23]. That is to say, regions within the CI distance are not counted (i.e., $n_0 = 0$). An example of the straight line and CI region is given in Fig. 1(c).

B. The AMPLE Model

By further considering the propagation carrier frequency as a factor, the decibel path loss of the zth T-R link can be expressed as [14], [23], [24]

$$\begin{aligned} \mathrm{PL}_z\,[\mathrm{dB}] = A + \sum_{r=1}^{R_z} 10 n_r \log_{10}\left(\frac{\sum_{k=0}^{r} d_k}{\sum_{k=0}^{r-1} d_k}\right) + p_z X \\ + 10\gamma \log_{10}(f_z) + \Psi_\sigma, \end{aligned} \tag{2}$$

where A, R_z, n_r, d_k, p_z, X, γ, f_z, and Ψ_σ are characterized as follows.

- ***Intercept*** (A): Within the straight line, A is the decibel path loss of the CI region.
- ***Intersected Regions*** (R_z & n_r): R_z regions in total are intersected within the zth T-R straight line, and n_r is the rth region PLE. Note that for different T-R pairs, R_z may be different as well.
- ***Weighted Path Loss*** (d_k): The weighted path loss of the rth region is computed by the subtraction between the end point path loss of rth and $r-1$th region, respectively [14], [23], [24]. Note that d_k is the kth region length.
- ***Penetration Loss*** (p_z & X): We assume that there are two penetrations when the straight line intersects a building, each with an associated penetration loss X. For the zth T-R link, p_z penetration losses are recorded along the straight line. Note that penetrations only exist when buildings are present (i.e., $p_z = 0$ if the scenario contains no buildings), as shown in Fig. 2.
- ***Frequency*** (γ & f_z): Based on the typical path loss characterization methods [4], [5], [6], [22], we add a coefficient γ to indicate the dependence of path loss on frequency [22], where f_z denotes the carrier frequency of the zth link in GHz.
- ***Shadowing*** (Ψ_σ): Ψ_σ is a normally distributed shadowing term with $N[0, \sigma^2]$ under dB-scale.

By combining terms with the same PLE, (2) can be simplified as region-type-based, which can be expressed as

$$\mathrm{PL}_z\,[\mathrm{dB}] = A + \sum_{m=1}^{M} D_m n_m + p_z X + 10\gamma \log_{10}(f_z) + \Psi_\sigma, \tag{3}$$

where M is the number of region types within the environment (e.g., $M = 4$ in Fig. 1(c)), n_m is the mth region type PLE, and D_m is the corresponding coefficient extracted by combining terms of n_m.

III. Ranplan Professional Ray-Tracing Simulations

In this section, we first introduce the current usage of ray-based simulations and the measurement-validated Ranplan Professional simulator. We then provide details of simulations for the UMa and UMi scenarios using Ranplan Professional. Following that, we give a simple validation of the collected dataset by extracting model parameters such as PLE and comparing them to those obtained from measurements in [22].

A. Ranplan Professional Ray-Tracing Simulator

With the development of ray-tracing technology, powerful ray-tracing simulators are used for hardware testbeds evaluations [26], [27], [28], essential 5G technology validations [29], channel model characterizations [30], and so on. These simulators have also been regarded as an alternative data collection method beyond hardware measurements due to their ability to collect larger data volume while with minor discrepancy with hardware measurement, and is called as "ray-tracing

TABLE I
ELECTROMAGNETIC PROPERTY OF MATERIALS USED IN RANPLAN PROFESSIONAL, INCLUDING LOSSES [DB] OF TRANSMISSION, REFLECTION, AND DIFFRACTION [41], [42], [43]

Object	Material	Transmission			Reflection			Diffraction		
		0.85 GHz	2.1 GHz	5 GHz	0.85 GHz	2.1 GHz	5 GHz	0.85 GHz	2.1 GHz	5 GHz
Building	Concrete	10.11 dB	20.25 dB	44.35 dB		6.00 dB		10.26 dB	18.37 dB	38.00 dB
Body of water	Water	16.16 dB	25.92 dB	49.09 dB		1.95 dB		6.00 dB	14.00 dB	33.00 dB
Foliage	Tree	0.10 dB/m	0.30 dB/m	0.60 dB/m		10.20 dB		-	-	-

measurements" [31]. In other words, for characterization of channel models, the database can be collected not only from hardware measurements, but also the ray-tracing simulations generated through reliable simulators. In this article, we use Ranplan Professional [32], a powerful commercial ray-tracing simulator, to characterize and validate the AMPLE model from 0.85 to 5 GHz. Validated by hardware measurements [33], [34], Ranplan Professional has been used to characterize propagation models [23], [35] and support other research in wireless communications [36], [37], [38], [39].

For the model characterization and validation, we focus on the UMa and UMi for outdoor scenario types. We consider the 5GNR system frequency bands at 0.85 GHz (5GNR band n5 with 10-MHz bandwidth), 2.1 GHz (5GNR band n1 with 10-MHz bandwidth), and 5 GHz (5GNR band n46 with 10-MHz bandwidth) across both scenario types, and we set up the simulation resolutions as 5 m. An example of the outdoor environment simulation is given in Fig. 3, and the detailed propagation information for each scenario simulation is given as follows.

B. UMa Simulations in Sheffield and Barnsley

For the UMa scenarios, we consider two outdoor simulations that are Sheffield and Barnsley in the U.K. Both Sheffield and Barnsley are the typical European style cities that have medium population and building densities. We first import the city layout from EDINA's Digimap Ordnance Survey [40], and we focus on the key environment regions that are general in real-world outdoor scenarios while have a significant impact on radio propagation. Those environment regions including *buildings*, *open space*, *foliage*, and *bodies of water* (lake, river, etc.). The electromagnetic properties of materials used in the simulations, including material type, transmission loss, reflection loss, and diffraction loss, are listed in Table I. The properties of concrete are derived from measurements conducted by Ranplan Wireless as part of the European project "Wireless Friendly and Energy Efficient Buildings (WiFEEB)" [41], and the properties of bodies of water and foliage are informed by [42], [43]. Note that, in order to the common use of the final model and the simplification of simulations, we here does not consider adding details into the outdoor scenario, such as road signs and other substances that are different in various places and are negligible in comparison to those key regions we covered [14]. Within the simulations, regions of the same type (e.g., buildings) are assumed to have consistent material properties and heights. Following that, we set foliage with a height of 10 m, and the buildings are made of heavy concrete with a height of 20 m, which is close to the average height in the typical UMa scenarios [4], [22]. For the scenario in Sheffield, it is bounded by latitudes and longitudes ranging from 53.36590854 to 53.39712604, and -1.5114482 to -1.46115222, respectively. In the meantime, the scenario in Barnsley is bounded by latitudes and longitudes ranging from 53.54123619 to 53.56927884, and -1.50333959 to -1.4537181, respectively.

Beyond that, the transmitters (Txs) in both scenarios are equipped with omnidirectional antennas transmitting at 5GNR frequencies of 0.85 GHz, 2.1 GHz, and 5 GHz as previously mentioned, with heights of 30 m [22]. For the exact positions, the Tx in Sheffield is positioned on the rooftop of a building at (53.381029, -1.4864733), and the Tx in Barnsley is positioned on the rooftop of a building at (53.5551977, -1.4789376). Along with that, the receiver (Rx) is positioned at a height of 1.5 m with the 5-meter resolution across the whole outdoor scenarios. The Tx power is set as 26 dBm, and both Tx and Rx are with 0 dBi antenna gains and with 0 dB cable loss. Based on the environments we set up, we collect a maximum of 823,923 raw data points from Sheffield and 682,803 raw data points from Barnsley across three carrier frequencies.

C. UMi Simulations in London and Manchester

For UMi scenarios, we simulate London and Manchester in the U.K., which are two typical European style UMi cities. We focus on the center of two cities (i.e., London Soho and the center of Manchester), that are with high building densities and street canyons. The construction process explained in the UMa scenarios (i.e., Section III-B) is used to set up the environments in two UMi cities (e.g., city layout and environment regions), except that the average building height is set to 10 m [4], [22]. The scenario in London is bounded by latitudes and longitudes ranging from 51.48038 to 51.51303 and -0.16366 to -0.11336, respectively. Also, for scenario in Manchester, it is bounded by latitudes and longitude ranging from 53.47072 to 53.4978 and -2.27098 to -2.21759, respectively.

For propagation information, the Txs in UMi scenarios have heights of 15 m (i.e., on the rooftop of a building), with the Tx in London positioned at (51.49474159, -0.14394048), and the Tx in Manchester positioned at (53.48710645, -2.24311856). Other propagation details, such as frequencies, Rx height, Tx power, and so on, are similar to those in the UMa scenarios. Due to the constraints of the UMi scenario, the overall signal coverage is significantly smaller than that of the full simulated

TABLE II
PARAMETERS OF THE CI PATH LOSS MODEL EXTRACTED FROM RANPLAN PROFESSIONAL SIMULATIONS AND MEASUREMENTS IN [22, TABLE I]. # OF DATA POINTS REFERS TO THE NUMBER OF DATA POINTS AFTER DISTANCE BINNING AND PATH LOSS THRESHOLDING

Scenario	Environment	Frequency [GHz]	Model	d_0 [m]	Data Source	# of Data Points	PLE	σ [dB]
UMa	LOS	5GNR 2.1	CI	1	Ranplan Professional	12,283	2.26	5.06
		2			Theodore S. Rappaport [22, Table I]	253	2.00	1.70
	NLOS	5GNR 2.1	CI	1	Ranplan Professional	211,996	2.92	10.08
		2			Theodore S. Rappaport [22, Table I]	583	2.80	3.50
UMi	NLOS	5GNR 2.1	CI	1	Ranplan Professional	27,619	2.62	10.31
		2.9			Theodore S. Rappaport [22, Table I]	18	2.90	2.90

environment in both cases. Finally, we collect 482,403 raw data points from London and 482,403 raw data points from Manchester across three carrier frequencies.

D. Validation Based on CI Model PLE Extraction

For path loss model characterization, a reliable dataset can produce similar model parameters (e.g., model PLE) compared to the PLEs obtained from measurements under similar propagation conditions recognized by professionals [4], [6], [22]. Under this way, to validate the simulation results for two scenario types, we compare the CI model parameters extracted from Ranplan Professional and measurements reported by the research group of Theodore S. Rappaport in [22] (UMa scenario in Aalborg, Denmark, and UMi scenario in New Jersey, USA). In other words, after filtering the simulation data points, we first extract the CI model parameters by the same closed-form solutions as shown in [22, Appendix Eq. (30) & (31)], and we compared the CI values that are extracted by measurements in [22, Table I]. Detailed process is given as follows. Note that for the CI model, it can be expressed as [22]

$$\begin{aligned} \mathrm{PL}_z^{\mathrm{CI}}(f_z, d_z)\,[\mathrm{dB}] &= A(f_z, d_0)\,[\mathrm{dB}] \\ &\quad + 10n\log_{10}(\frac{d_z}{d_0}) + \Psi_\sigma^{\mathrm{CI}}, \qquad d_z \geq d_0, \end{aligned} \tag{4}$$

with

$$A(f_z, d_0)\,[\mathrm{dB}] = 20\log_{10}\left(\frac{4\pi f_z d_0 \times 10^9}{c}\right), \tag{5}$$

where $A(f_z, d_0)$ is the free-space path loss in decibels with distance d_0 at carrier frequency f_z in GHz, n is the CI PLE, and $\Psi_\sigma^{\mathrm{CI}}$ is the shadowing term with $N[0, \sigma^2]$ under dB-scale.

To compare with the measurements around 2 GHz in [22], we combine all data points for each scenario type, filter the interference points (e.g., data points beyond a path loss value, such as 150 dB; data points beyond a T-R distance, such as 1.5 km for the UMa scenario, etc.) and extract the path loss data at 5GNR 2.1 GHz. After that, we classify the data points into LOS and NLOS sets based on map information, which is similar to the classification method in [22]. By using closed-form solutions for CI PLE n and standard deviation σ [22, Appendix Eq. (30) & (31)], we extract those values under the UMa LOS, NLOS, and the UMi NLOS, and compared with those extracted from measurements in [22], which are shown in Table II.

Throughout Table II, the CI PLE n extracted from Ranplan Professional are close to those in [22], with a maximum difference below 0.3, whereas the differences of standard deviation σ are large. The reasons of such differences including n and σ can be probably explained as:

- **Number of data points**: As shown in Table II, the number of data points exhibits significant discrepancies between Ranplan Professional simulations and measurements in [22], with a maximum difference exceeding 1,500 fold. A larger number of data points is more likely to result in a higher variance in distribution, leading to an increased σ. Despite this, the PLE values of the two remain close, indicating a high similarity in the path loss trend between simulations and measurements.
- **Frequency**: Differences between propagation carrier frequencies have a non-negligible impact on path loss, which further influences the model values. For example, as shown in the UMi NLOS case, the frequency difference (i.e., a 0.8-GHz difference) is one of the factors contributing to the PLE variation between simulation and measurement.
- **Environment**: Even within the same scenario type, environmental differences may lead to minor variations of model values between different datasets.

Overall, the simulation datasets of Ranplan Professional show high similarity for the CI model PLEs in comparison to those in [22, Table I], and in this article, we use these datasets to characterize the AMPLE model.

IV. CHARACTERIZATION OF THE AMPLE MODEL AND PERFORMANCE RESULTS

In this section, we introduce the process of characterizing the AMPLE model based on Ranplan simulations which are presented in Section III. Following that, we briefly introduce the compared models and the considered performance metrics including the two metrics we defined. Finally, we analyze the results and give the characterization parameters of the AMPLE model under the UMa and UMi scenarios from 0.85 to 5 GHz.

A. Characterization Process of the AMPLE Model

As shown in Fig. 4, the characterization process of the AMPLE model based on Ranplan Professional can be split into three stages, that is, region classification and map-data combination, simulation data processing, and model constructions.

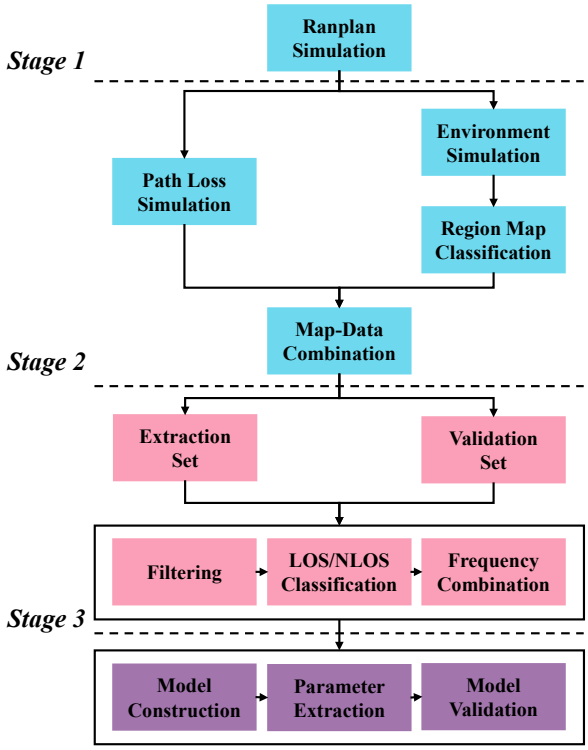

Fig. 4. Flowchart of characterization process based on Ranplan Professional simulations, similar process could be considered for other types of datasets.

Stage 1: Region Classification and Map-Data Combination. Initially, Ranplan Professional contains both environment simulation and the corresponding path loss simulations. Following the environment types we set up as described in Section III-B, we first extract the region maps of those scenarios from Ranplan Professional. By extracting Ranplan Professional simulations as extensible markup language (XML) files, we collect the 2D region maps of four simulated cities, which cover region types including *buildings*, *open space*, *foliage*, and *bodies of water*. To map the path loss data with the generated region maps, we consider the geographical coordinates of the simulated scenarios. That is, by adding latitude/longitude to region maps, each path loss data can be therefore mapped into the region map. The region maps of four scenarios with coordinates are shown in Fig. 5.

Stage 2: Data Processing. To characterize and validate the AMPLE model, the datasets of four cities are split into extraction and validation sets, where an *extraction set* refers to dataset used for model extraction, and a *validation set* refers to dataset used for validating the model performance. We take Sheffield in the UMa and Manchester in the UMi as extraction set for parameter extraction, and Barnsley in the UMa and London in the UMi as validation set for model validation. Following the similar filtering and LOS/NLOS classification strategy described in Section III-D, we combine three frequencies together for model characterization, where the detailed information is listed in Table III.

Stage 3: Model Extraction. Considering the straight line method described in Section II, we construct the model format in (3) for each T-R pair. Based on the statistical properties of path loss and shadowing, we extract the desired model parameters including PLEs n_m, intercept A, penetration loss X, frequency coefficient γ, and the standard deviation σ. Detailed extraction process is described in Appendix A.

B. Compared Models

To validate the performance of the AMPLE model, we consider a comparison with other path loss models, including the 3GPP path loss models, the 5GCMSIG CI model (i.e., CI-5GCMSIG), the 5GCMSIG ABG model (i.e., ABG-5GCMSIG), the CI model with extraction-set-based calibration (i.e., CI-Calibrated), and the ABG model with extraction-set-based calibration (i.e., ABG-Calibrated). The 3GPP and 5GCMSIG path loss models are respectively shown in [4, Table 7.4.1-1] and [6, Table6], and for the CI-Calibrated and ABG-Calibrated models, the calibration process is given as follows.

As shown in (4) and (5), the CI model can be expressed as [6], [22]

$$\mathrm{PL}_z^{\mathrm{CI}}(f_z, d_z)\,[\mathrm{dB}] = 20\log_{10}\left(\frac{4\pi f_z \times 10^9}{c}\right) + 10n\log_{10}\left(\frac{d_z}{1\,\mathrm{m}}\right) + \Psi_\sigma^{\mathrm{CI}}. \tag{6}$$

Based on the extraction set for the UMa/UMi scenarios and LOS/NLOS environments, we construct the CI-Calibrated model using the same method employed to characterize the AMPLE model, and the details are given in the Appendix B. Note that the initial values for the extraction are based on [6, Table 6].

Meanwhile, for the ABG model, it can be expressed as [6], [22]

$$\mathrm{PL}_z^{\mathrm{ABG}}(f_z, d_z)\,[\mathrm{dB}] = 10\alpha\log_{10}\left(\frac{d_z}{1\,\mathrm{m}}\right) + \beta + 10\gamma^{\mathrm{ABG}}\log_{10}\left(\frac{f_z}{1\,\mathrm{GHz}}\right) + \Psi_\sigma^{\mathrm{ABG}}, \tag{7}$$

where α is the model PLE, β is the intercept, and γ^{ABG} is the frequency coefficient. Since [6, Table 6] does not include the LOS environment for the UMa and UMi scenarios, the initial values for the LOS and NLOS environments in model extraction are based on [22, Table III] and [6, Table 6], respectively. Similar to the CI-Calibrated model, the details of calibration process are provided in Appendix C.

C. Performance Metrics

For performance metrics, we consider the RMSE and MAE to assess the point-wise performance of model, and the average total hit ratio error (AHRE) to evaluate prediction quality of path loss [44], [45], [46]. Furthermore, we define the PMDE to evaluate the overall alignment between prediction and measurement via statistical distributions, and the mean simulation time per data point to measure model complexity.

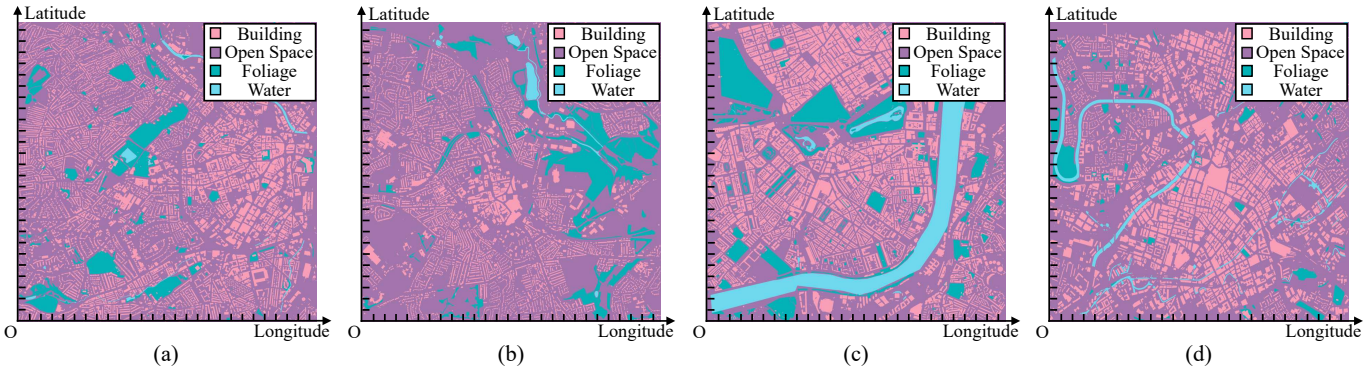

Fig. 5. Region maps of (a) Sheffield, (b) Barnsley, (c) London, and (d) Manchester. Along with the classified region types and the geographic coordinates.

Point-Wise Evaluation. For RMSE, it can be computed as

$$\text{RMSE} = \sqrt{\sum_{z=1}^{Z} \frac{(\hat{l_z} - l_z)^2}{Z}}, \tag{8}$$

where Z is the total number of data points, $\hat{l_z}$ is the zth predicted path loss, and l_z is the zth simulated path loss. For MAE, it can be expressed as

$$\text{MAE} = \sum_{z=1}^{Z} \frac{|\hat{l_z} - l_z|}{Z}. \tag{9}$$

Quality Evaluation. For AHRE [45], it is defined based on the total hit rate (THR) [44]. For THR, given a path loss threshold L_T, a prediction is considered correct if both the predicted path loss value $\hat{l_z}$ and the simulated/measured path loss value l_z are either greater than, less than, or equal to L_T, regardless of the deviation between $\hat{l_z}$ and l_z [46]. The AHRE represents the average deviation from 100% THR and is defined as [44], [45], [46]

$$\text{AHRE} = \frac{1}{N_{L_T}} \sum_{L_T = L_{T,\min}}^{L_{T,\max}} (100\% - \text{THR}(L_T)), \tag{10}$$

where N_{L_T} is the number of THR points, L_T is the path loss threshold. In this article, we set $L_{T,\min} = 80$ and $L_{T,\max} = 100$ for LOS environments, and $L_{T,\min} = 100$ and $L_{T,\max} = 120$ for NLOS environments in both the UMa and UMi scenarios, as most path loss values are concentrated within these ranges. Additionally, this method is useful for evaluating the validity of a model in cases where coverage is defined solely by a threshold value. Note that a smaller AHRE indicates better model prediction accuracy [44], [45], [46].

Overall Alignment Evaluation. To evaluate the model performance from a more comprehensive perspective, we define the prediction-measurement distribution error (PMDE) as an overall alignment metric. We first use the Akaike information criterion (AIC) to determine the best-fit distributions for both the predicted and measured (or simulated) datasets [47]. We here consider the candidate distributions including normal, lognormal, gamma, Weibull, Rayleigh, Ricean, and chisquare. By constructing the probability density functions (PDFs) for the two datasets, we then compute PMDE as the integral of the absolute difference between the two PDFs. The PMDE can be given as

$$\text{PMDE} = \int_x |f_{\text{p}}(x) - f_{\text{r}}(x)| dx, \tag{11}$$

where $f_{\text{p}}(x)$ and $f_{\text{r}}(x)$ are the PDFs of the predicted and measured (or simulated) datasets, respectively. Note that these two PDFs describe the overall distributions of the datasets across the environment, which is fundamentally different from point-based shadow fading that characterizes local variations at one fixed location [20].

The PMDE provides a statistically grounded way to evaluate the alignment between model-predicted and measured (or simulated) dataset distributions, going beyond point-wise errors and offering a distribution-level performance metric. Similar

TABLE III
INFORMATION OF DATASETS FOR MODEL EXTRACTION AND PERFORMANCE VALIDATION. # OF DATA POINTS REFERS TO THE NUMBER OF DATA POINTS AFTER DISTANCE BINNING AND PATH LOSS THRESHOLDING

Scenario	City	Set Type	Environment	Frequency Range [GHz]	# of Data Points	Distance Range [m]
UMa	Sheffield	Extraction	LOS	0.85-5	26,730	30-800
			NLOS		373,570	35-1,500
	Barnsley	Validation	LOS	0.85-5	36,331	31-800
			NLOS		391,134	31-1500
UMi	Manchester	Extraction	LOS	0.85-5	4,431	18-200
			NLOS		36,436	18-600
	London	Validation	LOS	0.85-5	3,396	28-200
			NLOS		37,109	28-600

TABLE IV
PERFORMANCE OF MODELS UNDER UMA BARNSLEY AND UMI LONDON FROM 0.85 TO 5 GHZ

Scenario	Environment	Metric	3GPP	CI-5GCMSIG	CI-Calibrated	ABG-5GCMSIG	ABG-Calibrated	AMPLE
UMa	LOS	RMSE [dB]	5.95	9.52	5.07	N/A	4.77	4.67
		MAE [dB]	4.58	8.10	4.23		3.88	3.68
		AHRE [%]	16.56	31.44	15.79		14.67	14.06
		PMDE	0.34	1.02	0.15		0.12	0.51
		t_p [ns]	110.51	13.12	12.91		12.46	9.00
	NLOS	RMSE [dB]	15.34	11.05	11.43	10.75	11.35	9.43
		MAE [dB]	12.91	9.47	9.81	9.12	9.63	7.81
		AHRE [%]	21.21	19.05	19.57	18.01	18.87	15.41
		PMDE	1.02	0.77	0.80	0.63	0.71	0.56
		t_p [ns]	117.40	15.45	15.49	13.26	13.41	11.4
UMi	LOS	RMSE [dB]	11.52	12.16	6.86	N/A	6.29	4.49
		MAE [dB]	10.71	11.39	5.78		5.02	3.65
		AHRE [%]	37.95	39.89	23.15		20.39	14.45
		PMDE	1.33	1.37	0.83		0.97	0.26
		t_p [ns]	117.01	25.44	24.88		24.84	25.12
	NLOS	RMSE [dB]	13.58	13.69	10.91	13.58	10.85	9.15
		MAE [dB]	11.54	11.71	8.17	11.54	7.93	6.54
		AHRE [%]	35.51	36.31	26.15	35.51	25.45	20.35
		PMDE	0.93	1.00	0.69	0.93	0.73	0.56
		t_p [ns]	130.65	13.47	13.48	13.44	12.95	9.95

to RMSE and MAE, PMDE is a general-purpose metric that can also be applied beyond path loss modeling, wherever distributional similarity between predictions and reference data is of interest. A smaller PMDE indicates a better alignment between prediction and measurement/simulation.

Complexity Evaluation. For the mean simulation time per data point, we run the models 1,000 times on the same dataset and compute the average simulation time for a single data point within one run. We define the mean simulation time per data point as

$$t_p = \frac{1}{CZ}\sum_{z=1}^{Z}\sum_{c=1}^{C} t_{z,c}, \tag{12}$$

where t_p represents the mean simulation time per data point, C is the total execution rounds (i.e., $C = 1000$ in this case), and $t_{z,c}$ denotes the simulation time of zth data point in the cth execution (or run) of the model. We perform multiple runs instead of a single run and simulate the entire dataset rather than individual data points to mitigate fluctuations in computer performance. In this article, we run the models and compute t_p on a typical office computer (central processing unit (CPU): Intel (R) Core (TM) i5-10505 3.20 GHz; random-access memory (RAM): 16.0 GB 2133 MHz) with MATLAB-R2024b programming environment.

D. Results and Analysis

As shown in Table IV, the performance of the models is evaluated using the metrics introduced in Section IV-C. Generally, the AMPLE model outperforms the current empirical path loss models used in the GSCMs [4], [6], while maintaining a same level of simulation time, that is, the same model complexity. Note that when computing the simulation time t_p in (12), similar to other empirical models, we consider the map information within the AMPLE model as pre-information (i.e., similar to simulated/measured path loss data) during model construction (as shown in Fig. 4 and explained in Section IV-A). Moreover, we draw the cumulative distribution functions (CDFs) to visualize the absolute error between the model predictions and the simulation results under two scenarios (i.e., $|\hat{l_z} - l_z|$), which are shown in Fig. 6 and Fig. 7.

For the UMa scenario under the LOS environment, the AMPLE model performs similarly to other models. This can be seen in both Table IV and Fig. 6(a), where the performance metrics in Table IV and the CDF plot in Fig. 6(a) show that the AMPLE model has similar performance compared to other models, such as the ABG-Calibrated model and the CI-Calibrated model. This is because the LOS case involves a simple environment where transmission experiences minimal environmental impact. In such a situation, considering environmental factors has limited contribution to path loss prediction. However, for the UMa scenario under the NLOS environment, environmental factors such as buildings and foliage cannot be ignored, making their consideration significant in path loss prediction [14], [23]. As shown in Table IV, the AMPLE model outperforms other models by considering main environmental factors, which provide more information during path loss predictions, and similar results can also be observed in Fig. 6(b). Meanwhile, in the more concentrated and complex UMi street canyon scenario, transmission is subject to greater environmental impacts, making environmental considerations even more crucial for path loss predictions. As a result, the AMPLE model outperforms other models, as shown in Table IV and Fig. 7.

Besides, to visually illustrate the performance of the AMPLE model, we present heatmaps and absolute error maps of the models under 0.85 GHz, as shown in Fig. 8 and Fig. 9 for the UMa and UMi scenarios, respectively. The absolute error map is computed based on the absolute error between the

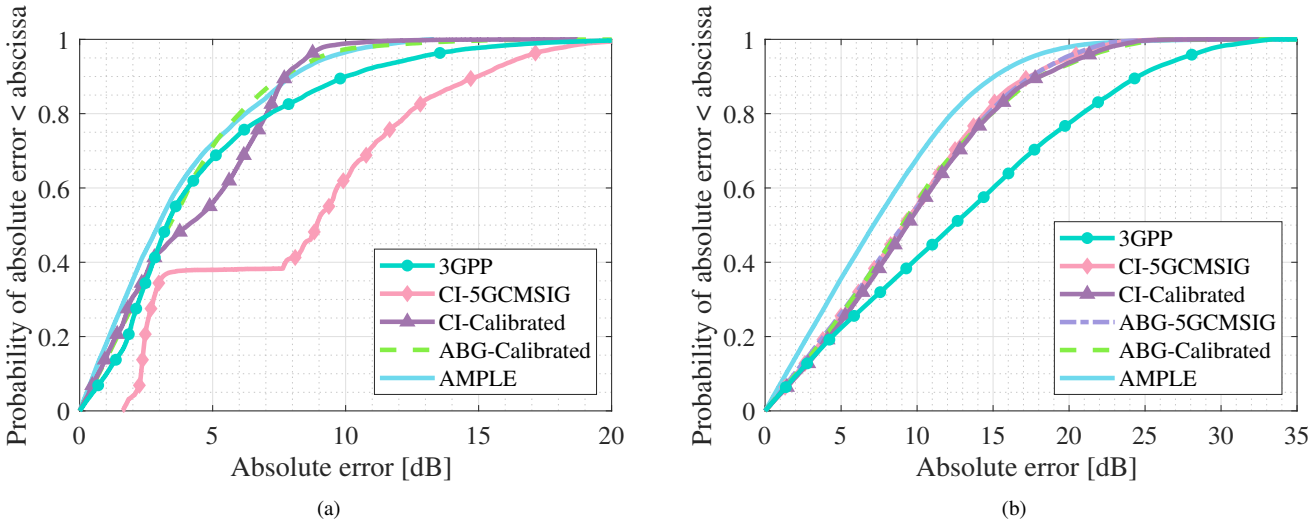

Fig. 6. CDF of absolute error between model predictions and Ranplan Professional simulations under the UMa Barnsley, with (a) LOS environment and (b) NLOS environment.

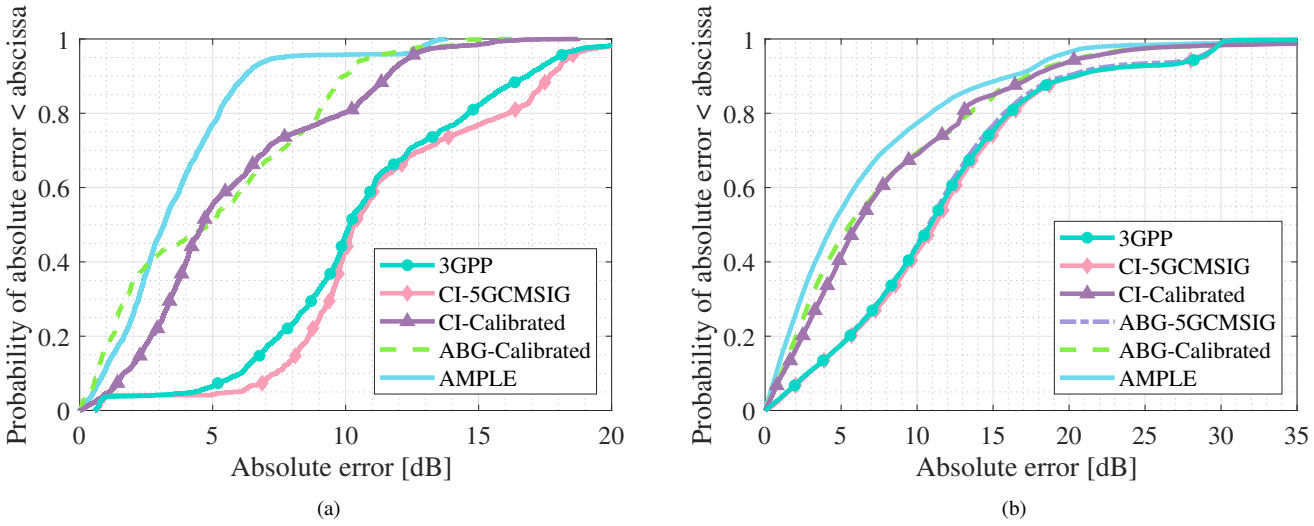

Fig. 7. CDF of absolute error between model predictions and Ranplan Professional simulations under the UMi London, with (a) LOS environment and (b) NLOS environment.

model predictions and Ranplan simulations. For the heatmaps in both scenarios (i.e., Fig. 8(b)-(g) and Fig. 9(b)-(g)), the predictions follow a radiation-like, distance-based trend under the LOS and NLOS cases, except that the AMPLE model predicts path loss based on both LOS/NLOS environments and environmental factors.

For the error maps in the UMa scenario (as shown in Fig. 8(h)-(m)), prediction accuracy is largely influenced by the environment. Taking the 3GPP model as an example (Fig. 8(h)), prediction errors are acceptable in the LOS environment but abruptly increase as the environment gradually transitions to the NLOS case. Even with different parameters for the NLOS environment [4, Table 7.4.1-1], the 3GPP model still has a mean error of around 12 dB. This is similar to the CI-5GCMSIG model (Fig. 8(i)) and the ABG-5GCMSIG model (Fig. 8(k)), both of which perform slightly better than the 3GPP model in the NLOS environment. We previously consider that this may be caused by the differences in model construction datasets, so we use Ranplan simulation data to calibrate both the CI model and the ABG model (details are provided in Section IV-B). However, as shown in Fig. 8(j) (the CI-Calibrated model) and Fig. 8(l) (the ABG-Calibrated model), the results indicate that calibration improves predictions only in LOS cases, while a gap remains in the NLOS case. Most errors are similar to those in the CI-5GCMSIG model and the ABG-5GCMSIG model, with a mean error of approximately 9 dB. Following that, by considering environmental factors, the AMPLE model (Fig. 8(m)) mitigates prediction errors in the NLOS case, with a mean error of around 8 dB.

For the error maps in the UMi scenario (as shown in Fig. 9(h)-(m)), prediction accuracy is influenced by both the environment and the dataset. The same environmental impact is observed in this scenario, where the 3GPP model (Fig. 9(h)), the CI-5GCMSIG model (Fig. 9(i)), and the ABG-5GCMSIG model (Fig. 9(k)) show significant prediction errors under the NLOS environment, with a mean error of approximately 12 dB. After calibration, the CI-Calibrated model (Fig. 9(j))

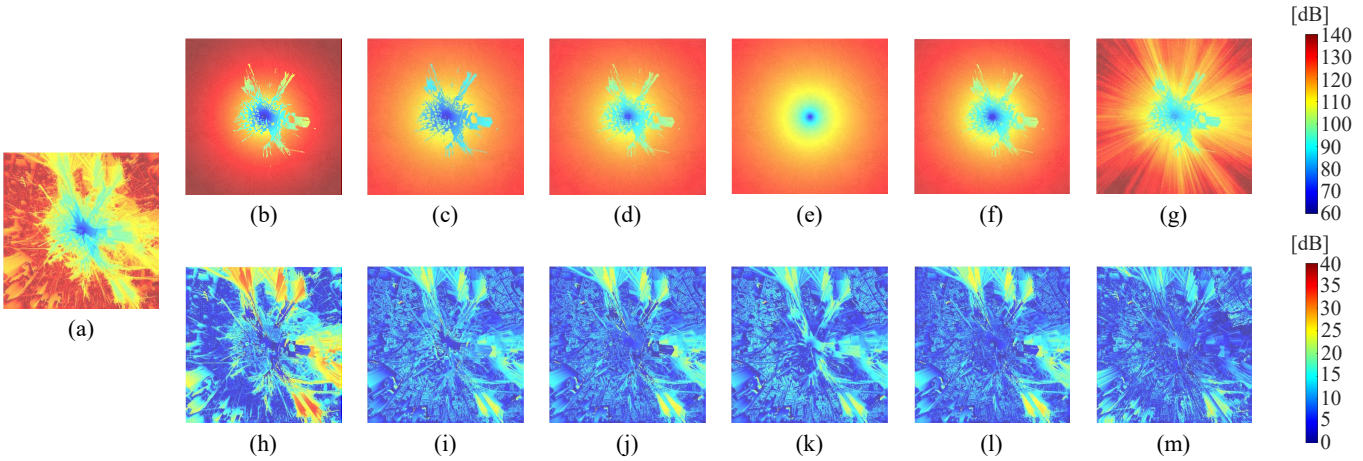

Fig. 8. Predictions under the UMa Barnsley 0.85 GHz, including: Heatmaps for (a) Ranplan Professional simulation, (b) 3GPP [4, Table 7.4.1-1], (c) CI-5GCMSIG [6, Table6], (d) CI-Calibrated, (e) ABG-5GCMSIG [6, Table6], (f) ABG-Calibrated, and (g) AMPLE; and absolute error maps for (h) 3GPP, (i) CI-5GCMSIG, (j) CI-Calibrated, (k) ABG-5GCMSIG, (l) ABG-Calibrated, and (m) AMPLE.

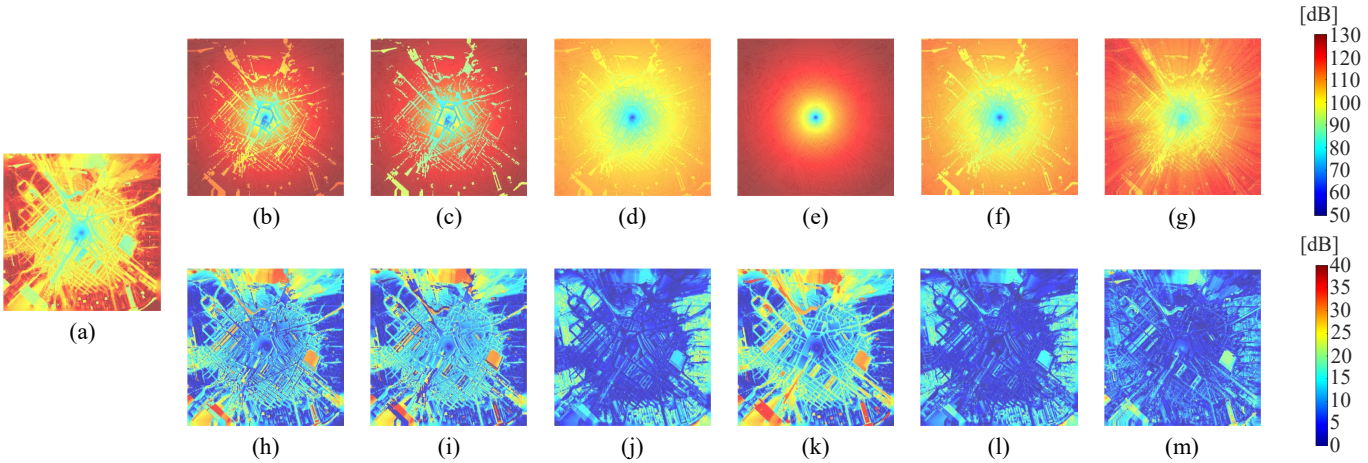

Fig. 9. Predictions under the UMi London 0.85 GHz, including: Heatmaps for (a) Ranplan Professional simulation, (b) 3GPP [4, Table 7.4.1-1], (c) CI-5GCMSIG [6, Table6], (d) CI-Calibrated, (e) ABG-5GCMSIG [6, Table6], (f) ABG-Calibrated, and (g) AMPLE; and absolute error maps for (h) 3GPP, (i) CI-5GCMSIG, (j) CI-Calibrated, (k) ABG-5GCMSIG, (l) ABG-Calibrated, and (m) AMPLE.

and the ABG-Calibrated model (Fig. 9(l)) show lower errors in the LOS environment but still have considerable errors in the NLOS environment, with a mean error of around 8 dB. Eventually, the environmental influences on predictions, especially in the NLOS environment, are effectively mitigated by the AMPLE model (Fig. 9(m)), with a mean error of around 7 dB.

E. The AMPLE model from 0.85 to 5 GHz

Table V lists the parameters of the AMPLE model for the UMa and UMi scenarios. With different antenna heights (i.e., UMa $h_{\mathrm{BS}} = 30$ m, and UMi $h_{\mathrm{BS}} = 15$ m), the intercept A in the UMa scenario is slightly larger than in the UMi scenario. Beyond that, since most environments consist of buildings and open space, the PLE values of these two region types (i.e., n_1 and n_2) along with the building penetration loss X largely influence the performance of the AMPLE model, resulting in distinct differences across environments/scenarios. In contrast, the PLEs of foliage and water (i.e., n_3 and n_4) remain similar across four cases. In the meantime, the frequency coefficient reflects the impact of frequency on path loss, where only the UMa LOS environment shows a weaker frequency dependence. This may arise from the simplicity of the environment [22] and the limited range of frequency bands, which prevents the full impact of frequency dependence from being observed. If more complex environments, more carrier frequencies, or both are contained in the datasets, the frequency dependence would increase.

Besides, two points require further clarification: (1) why the AMPLE model in the LOS environments still cover those environmental factors instead of modeling open space only, despite the typical definition of LOS; and (2) why the open space regions in the LOS environments of both scenarios have relatively lower PLE values. Regarding the first point, we classify data points based on both the map layout and a path loss threshold. That is, the LOS category includes not only direct line-of-sight links but also those with first-order reflections, which can still result in low path loss values [30]. Furthermore, according to the straight line mechanism described in Section II-A, all regions intersected by the straight line are considered to contribute partially to the total path

TABLE V
PARAMETERS OF THE AMPLE MODEL FOR UMA AND UMI FROM 0.85 TO 5 GHZ

Model Parameter	UMa		UMi	
	LOS	NLOS	LOS	NLOS
Intercept A	59.86	59.79	55.19	55.20
In-Building n_1	1.35	1.80	1.59	1.78
Open Space n_2	1.14	1.64	1.46	1.89
Foliage n_3	2.59	2.71	2.70	2.70
Bodies of Water n_4	1.79	1.93	1.80	1.80
Penetration X	0.09	0.28	0.18	0.17
Frequency Coefficient γ	0.92	1.94	1.97	1.98
Shadow Fading std. σ	5.40	9.53	8.01	8.00
Default Values	Frequency from 0.85-5 GHz, $h_{\text{BS}} = 30$ m, $h_{\text{UT}} = 1.5$ m		Frequency from 0.85-5 GHz, $h_{\text{BS}} = 15$ m, $h_{\text{UT}} = 1.5$ m	

loss of the link. Therefore, even in the LOS environments, the influence of environmental factors remains present in both scenarios.

Moreover, the low PLE value for open space within the LOS environment is also attributed to the model's mechanism. Since the Txs are placed on buildings and the environmental information is based on 2D maps, links without obstructions are consistently misrecognized as penetrating through at least one building (i.e., the one located beneath the Tx) before reaching the Rxs. In other words, the impact of open space tends to be underestimated because the model mistakenly attributes it to buildings — particularly in short-range LOS cases. Under these conditions, most of the open space influence is incorporated into the characterization of buildings, causing the PLE n_2 to remain low at 1.14 for the UMa LOS and 1.46 for the UMi LOS. Instead, due to the more complex region intersections in the NLOS environments, this type of misclassification has less impact, as reflected in the more realistic parameter values observed in the NLOS cases for both scenarios [4], [6]. While this misrecognition affects the PLE values in the LOS environments, it still results in good path loss prediction performance (as described in Section IV-D). Therefore, we consider addressing this issue as part of future work to further enhance the AMPLE model, particularly in the LOS environments.

V. DISCUSSION

A. Aim of the AMPLE Model

Over the past decade, research on statistical models has primarily focused on the practical applications of the CI, CIF, and ABG models, with various works including more deployment scenarios, sensitivity analyses, and so on. Still, the limitations of these models, as we discussed in the Introduction, have constrained further development in this field. Against this background, the AMPLE model is designed to enhance prediction accuracy within the structure of statistical models while maintaining low complexity. In other words, within the statistical model framework, we aim to strike a balance between providing practical model usages with a minimum of computational complexity and including as much detail as possible [25]. Using multiple PLEs and region maps, we link the environments with PLEs to capture the influences of different regions on a given link, thereby incorporating environmental information into the model. Subsequently, a straight-line method is employed to construct the model with low computational complexity. Overall, the AMPLE model builds a bridge between statistical path loss modeling and site-specific environment emulation [23], [48].

B. Further Usages of This Article

In this article, we enhance the AMPLE model with practical application by introducing a frequency-dependent coefficient (in Section II), which extend its applicability to multiple carrier frequencies. Also, we provide a standard model characterization process of the AMPLE model (in Section IV), which can be referred in the future AMPLE model design with variants.

For the extracted model parameters in Table V, they are derived from Ranplan simulations for UMa and UMi scenarios, where part of the simulations are initially compared with measurements reported by the research group of Theodore S. Rappaport in [22] (UMa scenario in Aalborg, Denmark, and UMi scenario in New Jersey, USA). The comparison is based on path loss modeling, where high-quality datasets tend to yield similar model parameters [4], [6], as illustrated in Section III-D. These parameters in Table V may be used to predict other UMa and UMi scenarios, or set as the initial parameters for model reconstruction by other datasets. That is to say, similar to the 3GPP model parameters [4], which serve as the basis for other models such as the 5GCMSIG [6] and mmMAGIC [10], the parameters in Table V can be regarded as reference values for constructing or fine-tuning the AMPLE model in future applications across different UMa and UMi areas.

Beyond the AMPLE model itself, the two novel metrics–PMDE for distributional alignment, and the mean simulation time per data point t_p for simulation complexity (as discussed in Section IV-C)–provide additional ways to evaluate model performance, not only for path loss models, but also for others.

C. Limitation and Future Works

Although the AMPLE model has been enhanced with a frequency coefficient in this article, there remain opportunities for additional improvements and refinements. Due to space constraints and the focused scope of this work, we briefly summarize the limitations and potential refinements of the AMPLE model.

2D Region Map to 3D Region Map. As we mentioned in Section IV-E, the misrecognition of buildings and penetrations near short-range in the AMPLE model is due to the limitation of 2D region maps. This can be addressed by introducing a 3D region map, that is, the heights of different region types, including buildings. By setting up region heights and 3D T-R distance, the straight-line method can accurately capture intersected regions, thereby eliminating misrecognitions such

as unintended building penetrations. This refinement would be particularly useful in scenarios such as high-rise urban canyons. Also, the PLE-region-type relationship would suffer less noise.

Frequencies, Mainstream Scenarios, and Measurements. For frequency bands, the current AMPLE model only covers 0.85-5 GHz, and more carrier frequencies must be considered to fulfill the requirements of path loss modeling in 6G or beyond. Also, since we follow the 3GPP channel model standard, which typically considers mainstream scenarios including UMa, UMi, rural macrocell (RMa), and indoor hotspot (InH), we here only cover part of the scenario types. Beyond that, this article is solely based on ray-based simulations, where future characterization of the AMPLE model should also consider measurements for more real scenarios and variations.

Others. For the AMPLE model, a typical problem, of which we simplified in this article, is the choice of region types within the initial model construction stage. Small region types, moving obstacles, and weather conditions also impact radio propagation and path loss, and can be considered for further improvement after the basic AMPLE model has been constructed. One potential method is to set up multiple levels of the AMPLE model to address the same scenario type with different environmental complexity. Beyond that, aspects such as model sensitivity, real-world deployment, and computational overhead in large-scale scenarios or multi-frequency scenarios, are unconsidered issues for the AMPLE model at the current stage. However, "first thing first", based on the authors' understanding, these issues are not of primary concern until the AMPLE model reaches a more mature stage of development.

VI. Conclusions

We have characterized the AMPLE model under the UMa and UMi scenarios from 0.85 to 5 GHz. By using Ranplan Professional, we simulated four cites to characterize and validate the AMPLE model. The ray-based simulations at 2.1 GHz are validated with measurements by extracting the CI model parameters and compared with those extracted from measurements in [22, Table I]. We also compared the AMPLE model with the 3GPP model, the ABG model, the CI model, and the models with simulation calibrations. The results showed that the AMPLE model outperforms these models by considering environments. Future works of the AMPLE model are mainly based on the discussions in Section V and also in [14] and [23].

Acknowledgment

The authors would like to thank Dr. Jiming Chen for the information on Ranplan Professional.

Appendix

We consider maximum likelihood with gradient descent to extract the parameters of the AMPLE model, the CI model, and the ABG model. The detailed extraction process for these three models are provided in this appendix.

A. The AMPLE Model

As shown in (3), the AMPLE model can be computed as

$$\mathrm{PL}_z\,[\mathrm{dB}] = A + \sum_{m=1}^{M} D_m n_m + p_z X + 10\gamma \log_{10}(f_z) + \Psi_\sigma. \quad (3)$$

With the random variable Ψ_σ, the path loss follows a normal distribution with $N[\mu(A, n_m, X, \gamma), \sigma^2]$, where [49]

$$\mu(A, n_m, X, \gamma) = A + \sum_{m=1}^{M} D_m n_m + p_z X + 10\gamma \log_{10}(f_z). \quad (13)$$

Following that, we first compute the PDF of (3), which can be expressed as

$$P(l_z; \mu(A,n_m, X, \gamma), \sigma) = \frac{1}{\sqrt{2\pi}\sigma} \exp\left(- \frac{(l_z - \mu(A, n_m, X, \gamma))^2}{2\sigma^2} \right), \quad (14)$$

where l_z is the zth path loss value. Then, the joint PDF (i.e., likelihood function) can be expressed as

$$F(\mu(A,n_m, X, \gamma), \sigma) = \prod_{z=1}^{Z} \frac{1}{\sqrt{2\pi}\sigma} \exp\left(- \frac{(l_z - \mu(A, n_m, X, \gamma))^2}{2\sigma^2} \right). \quad (15)$$

By converting the likelihood function F into its negative natural logarithm form, the problem of finding the optimal parameters can be formulated as minimizing this negative log-likelihood function, which can be expressed as

$$\arg \min_{\substack{A, n_m, \\ X, \gamma, \sigma}} (-\ln F(\mu(A, n_m, X, \gamma), \sigma)). \quad (16)$$

Since we use gradient descent to regress the parameters, the partial derivatives of $-\ln F(\mu(A, n_m, X, \gamma), \sigma)$ with respect to all parameters are required, including PLEs n_m, intercept A, penetration loss X, frequency coefficient γ, and the standard deviation σ, which are

$$-\frac{\partial \ln F(\mu(A, n_m, X, \gamma), \sigma)}{\partial A} = \sum_{z=1}^{Z} \left(\frac{\mu(A, n_m, X, \gamma) - l_z}{\sigma^2} \right), \quad (17)$$

$$-\frac{\partial \ln F(\mu(A, n_m, X, \gamma), \sigma)}{\partial n_m} = \sum_{z=1}^{Z} \left(\frac{(\mu(A, n_m, X, \gamma) - l_z) D_m}{\sigma^2} \right), \quad (18)$$

$$-\frac{\partial \ln F(\mu(A, n_m, X, \gamma), \sigma)}{\partial X} = \sum_{z=1}^{Z} \left(\frac{(\mu(A, n_m, X, \gamma) - l_z) p_z}{\sigma^2} \right), \quad (19)$$

$$-\frac{\partial \ln F(\mu(A, n_m, X, \gamma), \sigma)}{\partial \gamma} = \sum_{z=1}^{Z} \left(\frac{(\mu(A, n_m, X, \gamma) - l_z) 10 \log_{10}(f_z)}{\sigma^2} \right), \quad (20)$$

$$-\frac{\partial \ln F(\mu(A,n_m,X,\gamma),\sigma)}{\partial \sigma} = \sum_{z=1}^{Z}\left(\frac{1}{\sigma}-\frac{(l_z-\mu(A,n_m,X,\gamma))^2}{\sigma^3}\right). \tag{21}$$

Note that the initial values of gradient descent are chosen based on our previous works in [14], [23], and the step size is set as 2×10^{-6}.

B. The CI Model

As shown in (6), the CI path loss model can be expressed as [6], [22]

$$\mathrm{PL}_z^{\mathrm{CI}}(f_z,d_z)\,[\mathrm{dB}] = 20\log_{10}\left(\frac{4\pi f_z\times10^9}{c}\right) + 10n\log_{10}\left(\frac{d_z}{1\,\mathrm{m}}\right)+\Psi_\sigma^{\mathrm{CI}}. \tag{6}$$

With random variable $\Psi_\sigma^{\mathrm{CI}}$, the mean of the CI model is

$$\mu(n) = 20\log_{10}\left(\frac{4\pi f_z\times10^9}{c}\right)+10n\log_{10}(d_z). \tag{22}$$

Following that, the PDF of the CI model is

$$P(l_z;\mu(n),\sigma) = \frac{1}{\sqrt{2\pi}\sigma}\exp\left(-\frac{(l_z-\mu(n))^2}{2\sigma^2}\right). \tag{23}$$

By combining all data points, the likelihood function is written as

$$F(\mu(n),\sigma) = \prod_{z=1}^{Z}\frac{1}{\sqrt{2\pi}\sigma}\exp\left(-\frac{(l_z-\mu(n))^2}{2\sigma^2}\right). \tag{24}$$

Similarly, the parameters within the CI model can be treated as minimizing the negative natural logarithm of (24), which is

$$\arg\min_{n,\sigma}(-\ln F(\mu(n),\sigma)). \tag{25}$$

Therefore, the partial derivatives of $-\ln F(\mu(n),\sigma)$ including CI PLE n and standard deviation σ can be computed as

$$-\frac{\partial \ln F(\mu(n),\sigma)}{\partial n} = \sum_{z=1}^{Z}\left(\frac{(\mu(n)-l_z)10\log_{10}(d_z)}{\sigma^2}\right), \tag{26}$$

$$-\frac{\partial \ln F(\mu(n),\sigma)}{\partial \sigma} = \sum_{z=1}^{Z}\left(\frac{1}{\sigma}-\frac{(l_z-\mu(n))^2}{\sigma^3}\right). \tag{27}$$

We choose the initial values of both n and σ based on [6, Table 6], and the step size of gradient descent is set as 2×10^{-6}.

C. The ABG Model

As shown in (7), the ABG path loss model can be computed as [6], [22]

$$\mathrm{PL}_z^{\mathrm{ABG}}(f_z,d_z)\,[\mathrm{dB}] = 10\alpha\log_{10}\left(\frac{d_z}{1\,\mathrm{m}}\right)+\beta+10\gamma^{\mathrm{ABG}}\log_{10}\left(\frac{f_z}{1\,\mathrm{GHz}}\right)+\Psi_\sigma^{\mathrm{ABG}}. \tag{7}$$

With random variable $\Psi_\sigma^{\mathrm{ABG}}$, the mean of the ABG model is

$$\mu(\alpha,\beta,\gamma^{\mathrm{ABG}}) = 10\alpha\log_{10}\left(\frac{d_z}{1\,\mathrm{m}}\right)+\beta + 10\gamma^{\mathrm{ABG}}\log_{10}\left(\frac{f_z}{1\,\mathrm{GHz}}\right). \tag{28}$$

Following that, the PDF of the ABG model is

$$P(l_z;\mu(\alpha,\beta,\gamma^{\mathrm{ABG}}),\sigma) = \frac{1}{\sqrt{2\pi}\sigma}\exp\left(-\frac{(l_z-\mu(\alpha,\beta,\gamma^{\mathrm{ABG}}))^2}{2\sigma^2}\right), \tag{29}$$

Along with all data points, the likelihood function can be expressed as

$$F(\mu(\alpha,\beta,\gamma^{\mathrm{ABG}}),\sigma) = \prod_{z=1}^{Z}\frac{1}{\sqrt{2\pi}\sigma}\exp\left(-\frac{(l_z-\mu(\alpha,\beta,\gamma^{\mathrm{ABG}}))^2}{2\sigma^2}\right). \tag{30}$$

Similarly, the parameters within the ABG model can be formulated as minimizing the negative natural logarithm of (30), and can be expressed as

$$\arg\min_{\alpha,\beta,\gamma^{\mathrm{ABG}},\sigma}(-\ln F(\mu(\alpha,\beta,\gamma^{\mathrm{ABG}}),\sigma)). \tag{31}$$

In the meantime, the partial derivatives of $-\ln F(\mu(\alpha,\beta,\gamma^{\mathrm{ABG}}),\sigma)$ including PLE α, intercept β, frequency coefficient γ^{ABG}, and the standard deviation σ can be computed as

$$-\frac{\partial \ln F(\mu(\alpha,\beta,\gamma^{\mathrm{ABG}}),\sigma)}{\partial \alpha} = \sum_{z=1}^{Z}\left(\frac{(\mu(\alpha,\beta,\gamma^{\mathrm{ABG}})-l_z)10\log_{10}(d_z)}{\sigma^2}\right), \tag{32}$$

$$-\frac{\partial \ln F(\mu(\alpha,\beta,\gamma^{\mathrm{ABG}}),\sigma)}{\partial \beta} = \sum_{z=1}^{Z}\left(\frac{(\mu(\alpha,\beta,\gamma^{\mathrm{ABG}})-l_z)}{\sigma^2}\right), \tag{33}$$

$$-\frac{\partial \ln F(\mu(\alpha,\beta,\gamma^{\mathrm{ABG}}),\sigma)}{\partial \gamma^{\mathrm{ABG}}} = \sum_{z=1}^{Z}\left(\frac{(\mu(\alpha,\beta,\gamma^{\mathrm{ABG}})-l_z)10\log_{10}(f_z)}{\sigma^2}\right), \tag{34}$$

$$-\frac{\partial \ln F(\mu(\alpha,\beta,\gamma^{\mathrm{ABG}}),\sigma)}{\partial \sigma} = \sum_{z=1}^{Z}\left(\frac{1}{\sigma}-\frac{(l_z-\mu(\alpha,\beta,\gamma^{\mathrm{ABG}}))^2}{\sigma^3}\right). \tag{35}$$

For LOS and NLOS environments, the initial values are based on [22, Table III] and [6, Table 6], respectively. The step size of gradient descent is set as 2×10^{-6}.

REFERENCES

[1] J. Zhang *et al.*, "Channel measurement, modeling, and simulation for 6G: A survey and tutorial," 2023, arXiv: 2305.16616. [Online]. Available: https://arxiv.org/abs/2305.16616

[2] C.-X. Wang *et al.*, "6G wireless channel measurements and models: Trends and challenges," *IEEE Veh. Technol. Mag.*, vol. 15, no. 4, pp. 22–32, Dec. 2020.

[3] C.-X. Wang *et al.*, "A survey of 5G channel measurements and models," *IEEE Commun. Surv. Tutor.*, vol. 20, no. 4, pp. 3142-3168, 4th Quart., 2018.

[4] 3GPP, *Study on channel model for frequencies from 0.5 to 100 GHz, V16.1.0*, 2020. [Online]. Available: https://www.etsi.org

[5] 3GPP, *Spatial channel model for multiple input multiple output (MIMO) simulations, V11.0.0*, 2003. [Online]. Available: https://www.etsi.org

[6] NTT Docomo *et al.*, *5G channel model for bands up to 100 GHz, V2.0*, 2016. [Online]. Available: http://www.5gworkshops.com

[7] S. Jaeckel *et al.*, *QuaDRiGa—Quasi deterministic radio channel generator, user manual and documentation, V2.0.0*, 2017. [Online]. Available: https://quadriga-channel-model.de

[8] V. Nurmela *et al.*, *METIS channel models, Deliverable D1.4,* 2015. [Online]. Available: https://www.researchgate.net/publication/282807948

[9] P. Kyösti *et al.*, *WINNER II Channel Models, D1.1.2 V1.0*, 2007. [Online]. Available: http://www.signal.uu.se/Publications/WINNER/WINN2D112.pdf

[10] M. Peter *et al.*, *Measurement campaigns and initial channel models for preferred suitable frequency ranges, Deliverable D2.1,* 2016. [Online]. Available: https://ec.europa.eu/research/participants/documents/downloadPublic?documentIds=080166e5a7a6b182&appId=PPGMS

[11] S. Wu *et al.*, "A general 3-D non-stationary 5G wireless channel model," *IEEE Trans. Commun.*, vol. 66, no. 7, pp. 3065-3078, July 2018.

[12] ITU-R SG05, *Draft new report ITU-R m. [IMT-2020.eval]*, 2017. [Online]. Available: https://www.itu.int/md/R15-SG05-C-0057/en

[13] L. Liu *et al.*, "The COST 2100 MIMO channel model," *IEEE Wireless Commun. Mag.*, vol. 19, no. 6, pp. 92–99, Dec. 2012.

[14] L. Zhou *et al.*, "AMPLE: An adaptive multiple path loss exponent radio propagation model considering environmental factors," *IEEE Trans. Veh. Technol.*, vol. 74, no. 2, pp. 3395-3400, Feb. 2025.

[15] J. W. Schuster, and R. J. Luebbers, "Comparison of GTD and FDTD predictions for UHF radio wave propagation in a simple outdoor urban environment," in *Proc. IEEE Antennas Propag. Soc. Int. Symp. Dig.*, Montreal, QC, Canada, 1997, pp. 2022-2025.

[16] R. F. Harrington, *Field Computation by Moment Methods.* New Jersey, USA: Wiley, 1993.

[17] D. He *et al.*, "The design and applications of high-performance ray-tracing simulation platform for 5G and beyond wireless communications: A tutorial," *IEEE Commun. Surveys Tuts.*, vol. 21, no. 1, pp. 10–27, 1st Quart., 2019.

[18] G. Yu *et al.*, "A ray-launching algorithm for polarized wireless channel prediction," in *Proc. IEEE Glob. Commun. Conf. Workshops (GlobCom Wkshps)*, Kuala Lumpur, Malaysia, Dec. 4-8, 2023, pp. 1928-1933.

[19] A. Goldsmith, *Wireless Communications*. Cambridge, UK: Cambridge University Press, 2005.

[20] T. S. Rappaport, *Wireless Communications: Principles and Practice*. New Jersey, USA: Prentice Hall, 1996.

[21] S. I. Umana, N. O. Akpbio, and S. E. Mbong, "Stanford university interim propagation loss model for a gmelina arborea tree-lined road," *Rev. Comput. Eng. Res.*, vol. 5, no. 2, pp. 57–63, 2018.

[22] S. Sun, *et al.*, "Investigation of prediction accuracy, sensitivity, and parameter stability of large-scale propagation path loss models for 5G wireless communications," *IEEE Trans. Veh. Technol.*, vol. 65, no. 5, pp. 2843–2860, May 2016.

[23] L. Zhou *et al.*, "An environment-adaptive radio propagation path loss model with ray-based validation," *IEEE Antennas Wireless Propag. Lett.*, vol. 23, no. 10, pp. 3217-3221, Oct. 2024.

[24] J. Zhang *et al.*, "A method of fast path loss calculation considering environmental factors," International Patent WO2023/214176A1, Nov. 2023.

[25] V. Erceg *et al.*, "An empirically based path loss model for wireless channels in suburban environments," *IEEE J. Sel. Areas Commun.*, vol. 17, no. 7, pp. 1205–1211, July 1999.

[26] T. Kwon *et al.*, "RF lens-embedded massive MIMO systems: Fabrication issues and codebook design," *IEEE Trans. Microw. Theory Tech.*, vol. 64, no. 7, pp. 2256–71, July 2016.

[27] Y.-J. Cho *et al.*, "RF lens-embedded antenna array for mmWave MIMO: Design and performance," *IEEE Commun. Mag.*, vol. 56, no. 7, pp. 42–48, July 2018.

[28] B. Ai *et al.*, "On indoor millimeter wave massive MIMO channels: Measurement and simulation," *IEEE J. Sel. Areas Commun.*, vol. 35, no. 7, pp. 1678–1690, July 2017.

[29] Y.-G. Lim *et al.*, "Waveform multiplexing for new radio: Numerology management and 3D evaluation," *IEEE Wirel. Commun.*, vol. 25, no. 5, pp. 86–94, Oct. 2018.

[30] K. Guan *et al.*, "Channel characterization for intra-wagon communication at 60 and 300 GHz bands," *IEEE Trans. Veh. Technol.*, vol. 68, no. 6, pp. 5193-5207, June 2019.

[31] Y.-G. Lim *et al.*, "Map-based millimeter-wave channel models: An overview, data for B5G evaluation and machine learning," *IEEE Wireless Commun.*, vol. 27, no. 4, pp. 54–62, Aug. 2020.

[32] *Ranplan Professional*, 2025. [Online]. Available: https://www.ranplanwireless.com/products/professional

[33] W. Yang *et al.*, "Verification of an intelligent ray launching algorithm in indoor environments in the Ka-band," *Radio Sci.*, vol. 56, no. 9, pp. 1-11, Sept. 2021.

[34] W. Yang *et al.*,"Indoor measurement based verification of ray launching algorithm at the Ka-band," in *Proc. XXXIIIrd Gen. Assem. Sci. Symp. Int. Union Radio Sci. (URSI GASS)*, Rome, Italy, Aug. 29-Sept. 5, 2020, pp. 1-4.

[35] S. Bakirtzis *et al.*, "EM DeepRay: An expedient, generalizable, and realistic data-driven indoor propagation model," *IEEE Trans. Antennas Propag.*, vol. 70, no. 6, pp. 4140–4154, June 2022.

[36] J. Zhang *et al.*, "Spatial scattering modulation with multipath component aggregation," *IEEE Trans. Green Commun. Netw.*, vol.8, no. 1, pp. 18-34, Mar. 2024.

[37] J. Zhang *et al.*, "Performance evaluation of spatial scattering modulation in the indoor environment," in *Proc. Int. Symp. Wirel. Commun. Syst. (ISWCS)*, Hangzhou, China, Oct. 19-22, 2022, pp. 1-6.

[38] K. Qiu *et al.*, "Pseudo ray-tracing: Deep leaning assisted outdoor mm-wave path loss prediction," *IEEE Wireless Commun. Lett.*, vol. 11, no. 8, pp. 1699–1702, Aug. 2022.

[39] C. Qin *et al.*, "Simulation based channel hardening of cell-free massive MIMO in mm-wave," in *Proc. XXXIVth Gen. Assem. Sci. Symp. Int. Union Radio Sci. (URSI GASS)*, Rome, Italy, Aug. 28–Sept. 4, 2021, pp. 1–4.

[40] Ordnance Survey (GB), OS Open Map - Local [SHAPE geospatial data], Scale 1:10000, Tiles: se, Updated: 12 October 2023, Using: EDINA Digimap Ordnance Survey Service, Downloaded: Aug. 2024. [Online]. Available: https://digimap.edina.ac.uk

[41] J. M. Rigelsford *et al.*, *Wireless/Energy efficiency of typical building components and architecture, Deliverable D1.2*, 2013. [Online]. Available: https://cordis.europa.eu/project/id/286333/reporting/es

[42] ITU-R, *Electrical characteristics of the surface of the Earth*, 2021. [Online]. Available: https://www.itu.int/rec/r-rec-p.527/en

[43] ITU-R, *Attenuation in vegetation*, 2021. [Online]. Available: https://www.itu.int/rec/r-rec-p.833/en

[44] A. S. Owadally, E. Montiel, and S. R. Saunders, "A comparison of the accuracy of propagation models using hit rate analysis," in *Proc. 54th IEEE Veh. Technol. Conf. (VTC Fall)*, Atlantic City, NJ, USA, Oct. 7–11, 2001, pp. 1979-1983.

[45] E. Östlin, H. -J. Zepernick, and H. Suzuki, "Evaluation of the new semi-terrain based propagation model recommendation ITU-R P.1546," in *Proc. 58th IEEE Veh. Technol. Conf. (VTC Fall)*, Orlando, FL, USA, Oct. 6–9, 2003, pp. 114-118.

[46] E. Östlin, H.-J. Zepernick, and H. Suzuki, "Macrocell path-loss prediction using artificial neural networks," *IEEE Trans. Veh. Technol.*, vol. 59, no. 6, pp. 2735–2747, July 2010.

[47] R. Zhang *et al.*, "Measurement and modeling of angular spreads of three-dimensional urban street radio channels," *IEEE Trans. Veh. Technol.*, vol. 66, no. 5, pp. 3555–3570, May 2017.

[48] H. Gao *et al.*, "Digital twin enabled 6G radio testing: Concepts, challenges and solutions," *IEEE Commun. Mag.*, vol. 61, no. 11, pp. 88-94, Nov. 2023.

[49] C. Gustafson *et al.*, "Statistical modeling and estimation of censored pathloss data," *IEEE Wireless Commun. Lett.*, vol. 4, no. 5, pp. 569–572, Oct. 2015.